applied sciences

MDPI

Article

Effect of Initial Grain Size on Microstructure and Mechanical Properties of In Situ Hybrid Aluminium Nanocomposites Fabricated by Friction Stir Processing

Ghasem Azimiroeen [1,*], Seyed Farshid Kashani-Bozorg [2], Martin Nosko [3] and Saeid Lotfian [4,*]

[1] Centre of Engineering and Technical Skills Training, Isfahan University of Technology, Isfahan P.O. Box 84156-83111, Iran
[2] Centre of Excellence for Surface Engineering and Corrosion Protection of Industries, School of Metallurgy and Materials Engineering, College of Engineering, University of Tehran, Tehran P.O. Box 11155-4563, Iran; fkashani@ut.ac.ir
[3] Institute of Materials and Machine Mechanics, Slovak Academy of Sciences, Dúbravská Cesta 9, 845 13-11 Bratislava, Slovakia; martin.nosko@savba.sk
[4] Naval Architecture, Ocean and Marine Engineering Department, University of Strathclyde, Glasgow G1 1XQ, UK
* Correspondence: azimi_gh@iut.ac.ir (G.A.); saeid.lotfian@strath.ac.uk (S.L.)

Abstract: Friction stir processing (FSP) offers a unique opportunity to tailor the microstructure and improve the mechanical properties due to the combination of extensive strains, high temperatures, and high-strain rates inherent to the process. Reactive friction stir processing was carried out in order to produce in situ Al/($Al_{13}Fe_4$ + Al_2O_3) hybrid nanocomposites on wrought/as-annealed (673 K) AA1050 substrate. The active mixture of pre-ball milled Fe_2O_3 + Al powder was introduced into the stir zone by pre-placing it on the substrate. Microstructural characterisation showed that the $Al_{13}Fe_4$ and Al_2O_3 formed as the reaction products in a matrix of the dynamically restored aluminium matrix. The aluminium matrix means grain size was found to decrease markedly to 3.4 and 2 μm from ~55 μm and 40–50 μm after FSP using wrought and as-annealed substrates employing electron backscattered diffraction detectors, respectively. In addition, tensile testing results were indicative that the fabricated surface nanocomposite on the as-annealed substrate offered a greater ultimate tensile strength (~160 MPa) and hardness (73 HV) than those (146 MPa, and 60 HV) of the nanocomposite formed on the wrought substrate.

Keywords: AA1050; reactive friction stir processing; in situ nanocomposites; grain refinement; EBSD; annealing

Citation: Azimiroeen, G.; Kashani-Bozorg, S.F.; Nosko, M.; Lotfian, S. Effect of Initial Grain Size on Microstructure and Mechanical Properties of In Situ Hybrid Aluminium Nanocomposites Fabricated by Friction Stir Processing. *Appl. Sci.* **2023**, *13*, 7337. https://doi.org/10.3390/app13127337

Academic Editor: Victor Franco Correia

Received: 8 May 2023
Revised: 7 June 2023
Accepted: 14 June 2023
Published: 20 June 2023

1. Introduction

Friction stir processing (FSP) is a relatively new solid-state process adapted from friction stir welding (FSW) and has been explored to homogenise the microstructure and refine the grain size [1–4]. The efficient grain refinement during the FSP results from severe plastic deformation and dynamic recrystallisation [5]. During the last decade, the FSP has been considered to modify the microstructure and increase the mechanical strength of components made via various manufacturing processes, such as castings [6,7]. A critical advantage of utilising the FSP is introducing reinforcements particles in the metal matrix, resulting in refined microstructure and excellent mechanical properties [8–10]. Additionally, considering the simplicity of the process, FSP has the potential to be used for homogenisation, fabrication of fine-grained alloys, surface treatment, and fabricating the hybrid metal matrix composites [11–13]. All mentioned benefits, alongside the possibility of automation of the process, recently made the FSP a candidate to be used in remanufacturing [14].

Recently, considerable research has been done on strengthening the metal matrix with more than one reinforcing material in order to improve the properties of the matrix

metal/alloy [15,16]. These types of composites are called hybrid composites by various research scientists. Hybrid composites have shown better properties than composites reinforced with one kind of particle, as the advantages of different particles are combined [15–18]. FSP is one of the new methods to process these types of composites. Hybrid composites can be fabricated additively and in situ using the reactive FSP [15,16]. Chemical reactions between aluminium and suitable metal oxides have been utilised to produce in-situ hybrid composites by combining the FSP and the thermite reaction. The mechanical properties increase due to the formation of the fine microstructure and nanosized products after the reaction. Various aluminium-based hybrid nanocomposites have been fabricated by FSP using Al–Fe_2O_3 [19], Al–Fe_3O_4 [20], Al-TiO_2 [21,22], Al-CeO_2 [23], Al-SiC [24] and Al-CuO [25] systems, in which particles (e.g., Al_2O_3) are formed in situ by reactive mechanisms.

Various researchers have investigated mechanisms that lead to grain refinement during FSP. They concluded that severe deformation and high temperature during FSP lead to microstructure refinement [8]. Based on the literature review and our reported findings in this study, during the FSP, materials have been subjected to hot deformation, and as a result, dynamic recovery (DRV) and dynamic recrystallisation (DRX) of the highly distorted grains take place and cause grain refinements. It is worth noting that in materials with high stacking fault energy (SFE), such as aluminium, continuous dynamic recrystallisation (CDRX) is the mechanism of new grain formation [26,27]. The CDRX mechanism has been detected in some metals with high SFE, such as ferritic steels, β titanium alloys, and aluminium alloys [27].

New grains develop due to a gradual increase in misorientations between subgrains formed by plastic deformation [28]. Studies show that misorientation angles at subgrain boundaries developed near the primary grain boundary are larger than those within the grain and can quickly transfer to high-angle boundaries. This observation indicates that the grain boundaries are preferred as the nucleation sites for new grains. Therefore, metals with smaller primary grains must display greater kinetics for grain refinement during severe strain deformation. It should be noted that in addition to the initial microstructure, the presence of particles also affects the grain refinement rate [29]. Both inside and outside of the grains, these second-phase particles are dispersed throughout the matrix. The secondary particles pin grain boundaries, which may act as a source of concentrated stress and generate dislocations that result in the development of subgrains [30]. As mentioned, most metal parts are subjected to hot deformation during the FSP process, during which dynamic recrystallisation often occurs. The final microstructure and mechanical properties of alloys are primarily determined by recrystallisation and related annealing phenomena. Many factors can have a significant effect on DRX, which includes: the stacking fault energy, the thermo-mechanical processing (TMP) conditions, the initial grain size, and the amount and size of the second phase particles [31–33]. The initial grain size also plays a role in determining which type of dynamic recrystallisation process takes place during hot deformation. For example, decreasing the initial grain size from 35 μm to 8 μm leads to the transformation of DDRX to CDRX for 304 austenitic stainless steel [27].

In our previous works, we produced fabricated in situ Al/($Al1_3Fe_4$ + Al_2O_3) hybrid nanocomposites using reactive friction stir processing (FSP) by introducing Fe_2O_3 powder into the stir zone of rolled AA1050 aluminium alloy. The current work focuses on the effect of initial grain size on the final microstructure and mechanical properties of fabricated hybrid nanocomposites using reactive friction stir processing (FSP) from Al and Fe_2O_3 systems.

2. Materials and Methods

In the present research, the production of nanocomposite from the Fe_2O_3–Al system will be reported using FSP technology. The matrix alloy selected was a 5 mm thick commercial 1050 aluminium alloy plate. Table 1 indicates the typical chemical composition of the Al sheet. Both rolled and annealed plates were utilised for the FSP in order to study the

effect of the base metal microstructure on the microstructure of the friction stir processed composite (Figure 1).

Table 1. Nominal chemical composition of BM, 1050 aluminium alloy sheet (wt.%).

Al	Zn	Cr	Mg	Mn	Cu	Fe	Si
Balance	0.0097	0.0041	0.0017	0.0061	0.0123	0.272	0.206

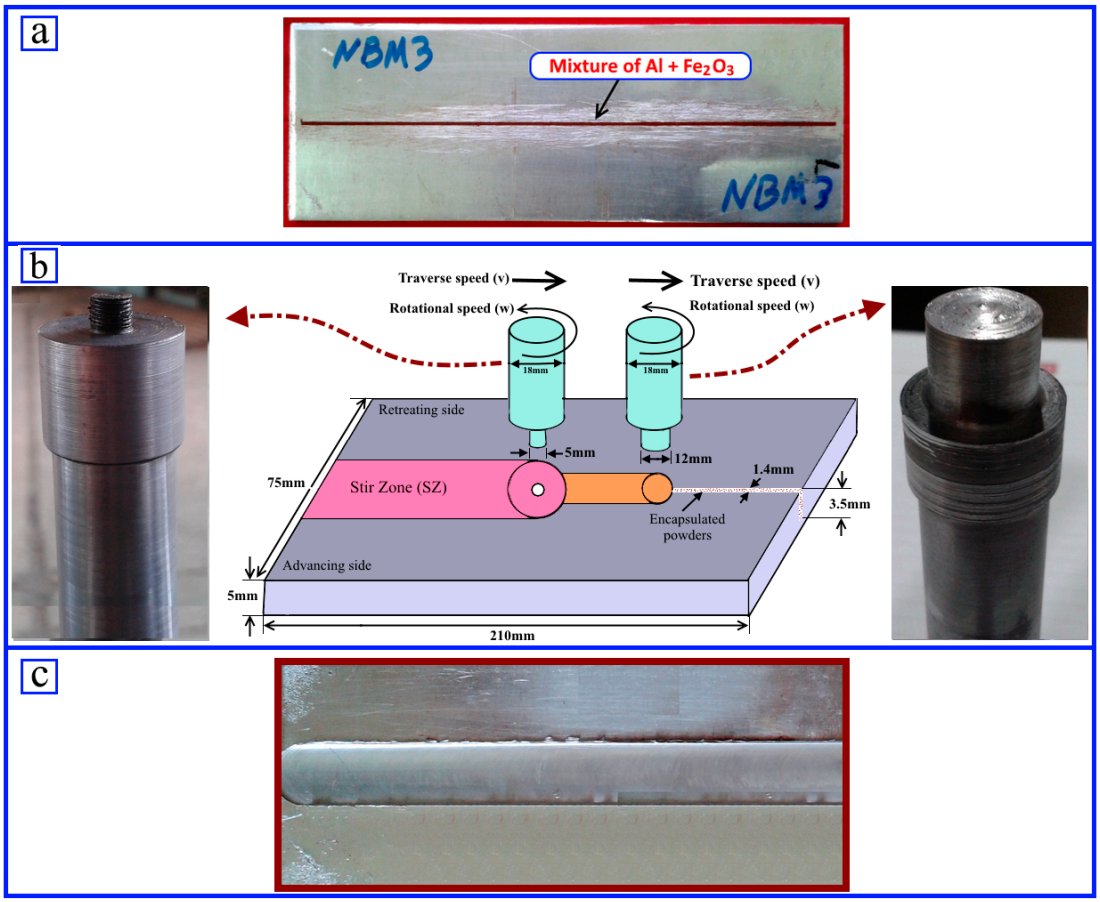

Figure 1. (**a**) Specimen preparation for the FSP, (**b**) schematic of FSP accomplishment and (**c**) the prepared nanocomposite from the top view.

Annealing was performed at 673 K for 3.5 h. The Al sheet was cut into pieces that measured 210 mm × 70 mm × 5 mm to prepare the workpieces, and a groove that was 1.4 mm wide and 3.5 mm deep was machined into the middle of the piece. The milled powder combination is next inserted into the groove that has been cut out. The stoichiometric compositions were used to prepare the powder mixture of Fe_2O_3 (>98% purity, the particle size of 1 µm) and Al (>99% purity, the average size of ~100 µm). The mixed powder was mechanically milled for two hours using a high-energy planetary mill under the argon atmosphere. The purpose of ball milling of the powder mixture before the FSP was to enhance the reaction rate during the FSP. FSP is performed rapidly after embedding the milled product in the created groove to avoid powder oxidation. The tracks filled with powder were FSPed, employing a vertical milling machine. The rotational tool speed and the traverse velocity were 1400 rpm and about 40 mm/min, respectively. Four FSP passes were carried out with 100% overlap. X-ray diffractometry (XRD), using a Philips X'Pert Pro unit, was used to determine the crystal structures of the top surfaces of the fabricated hybrid nanocomposites. The unit was equipped with monochromatic Cu-K_α radiation and

operated at a voltage and current of 40 kV and 30 mA, respectively. Employing a step size of 0.02° and time per step of 5 s, high-precision X-ray diffraction patterns were obtained.

Microstructural characterisation of the fabricated hybrid nanocomposites was carried out using optical (OM, Olympus GX51) and Jeol-JSM7600F field emission scanning electron microscopy (FESEM). The latter was operated at 20 kV and linked to an energy-dispersive spectrometer device (Bruker silicon drift detector) for point chemical analyses and X-ray mapping. Cross sections of the fabricated hybrid nanocomposites were prepared and polished according to the standard metallographic preparation. In addition, both secondary and backscattered electron imaging were obtained. Moreover, the electron backscattered diffraction (EBSD) examination was conducted using a plan-view cross-section of the fabricated hybrid nanocomposites. In this regard, the samples were automatically ground and polished, followed by colloidal silica polishing for 45 min to achieve high-quality surfaces for EBSD studies. HKL technology's Channel V software was used to process the data after it was created using the EBSD (OXFORD Instrument-X Max, Abingdon, UK) method, which was utilised to obtain electron channelling patterns using an ultra-sensitive CCD camera. Each EBSD map had a scanning step of 0.2 μm and an average confidential index that varied from 0.38 to 0.57. Using the Channel V software, the volume fraction of LAGBs and HAGs was calculated from the EBSD maps. The data analysis did not include below 2° misorientation at the grain boundary. High-angle boundaries (HABs) were defined using a 15° boundary misorientation. For TEM examinations, thin slices of the fabricated composites were cut from the middle part, measuring around 40 micrometres thick and 3 millimetres in diameter. Using a Gatan precision ion mill (Gatan PIPS II, Model 695), these sections were first dimpled with a Gatan dimpler and then thinned to electron transparency. Until the disc was perforated, ion milling was carried out at 5 keV and a 5° milling angle. The thin foil was examined Using a JEOL 2000 FX field emission (FE) TEM running at 300 kV when an EDS instrument was connected to TEM.

Gnehm FM 100 is used to obtain the microhardness profiles with an applied stress of 50 N and a dwell time of 10 s. The 0.5 mm intervals were considered during the hardness measurement to avoid any plastic deformation effect between the indentations. Additionally, the hardness measurements were done along a line 2.5 mm down from the top surface. Longitudinal tensile samples were prepared from the stir zone (SZ) of workpieces according to ASTM standard E8M with a gauge length of 25 mm. The mechanical properties of the specimens were evaluated on an Instron 5582 universal testing machine using an initial strain rate of 1×10^{-3} s^{-1}.

3. Results and Discussion

Figures 2 and 3 illustrate the Optical and EBSD images of as-received AA1100 (wrought alloy) and annealed Al alloy, respectively. As stated, the wrought alloy showed an elongated grain morphology (Figure 2a,b). In contrast to the wrought alloy, annealed specimen's initial microstructure consists of coarse equiaxed grains (Figure 3a,b) with an average size of ~40–50 μm. As can be seen, the fraction of the low-angle grain boundaries (LAGBs) is high for both samples (Figures 2c and 3c).

Optical micrographs of the rolled and the annealed specimens after FSP are shown in Figure 4. The stir zone (SZ) can be distinctly recognised from the base metal in both samples. As stated above, the base metal of rolled specimen consists of elongated grains in the rolling direction; in contrast, the annealed sample's base metal shows equiaxed grains. However, the SZs of both samples consist of extremely fine grains. The subsequent figures will demonstrate more detailed information on microstructural features (Figures 6–8).

Monitoring thermal histories during FSP is essential as these affect microstructural developments and mechanical characteristics. Figure 5 shows the temperature profiles during the fourth pass of FSP. The two curves experienced a similar pattern.

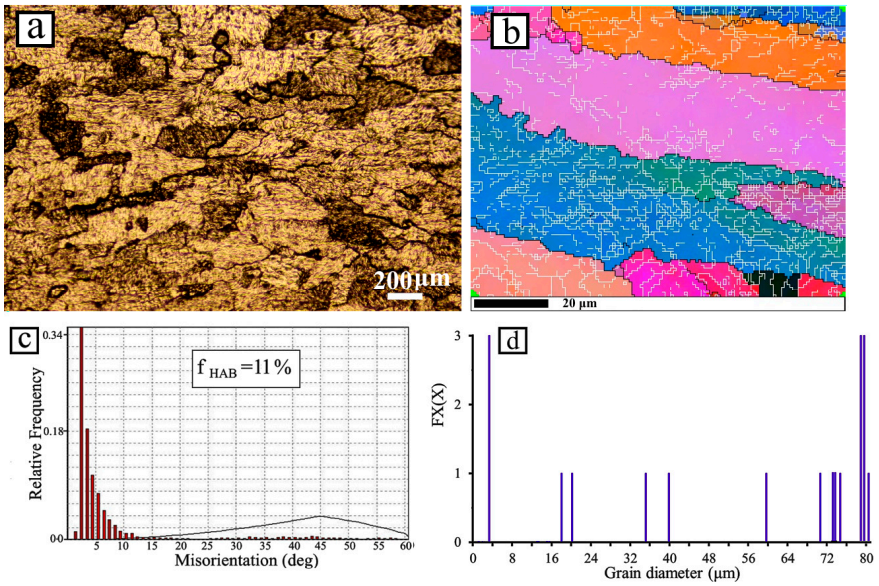

Figure 2. Optical micrographs (**a**), EBSD maps (**b**), high angle fraction diagrams (**c**), and grain size distribution (**d**) in as-received (wrought alloy) AA1100 aluminium alloy.

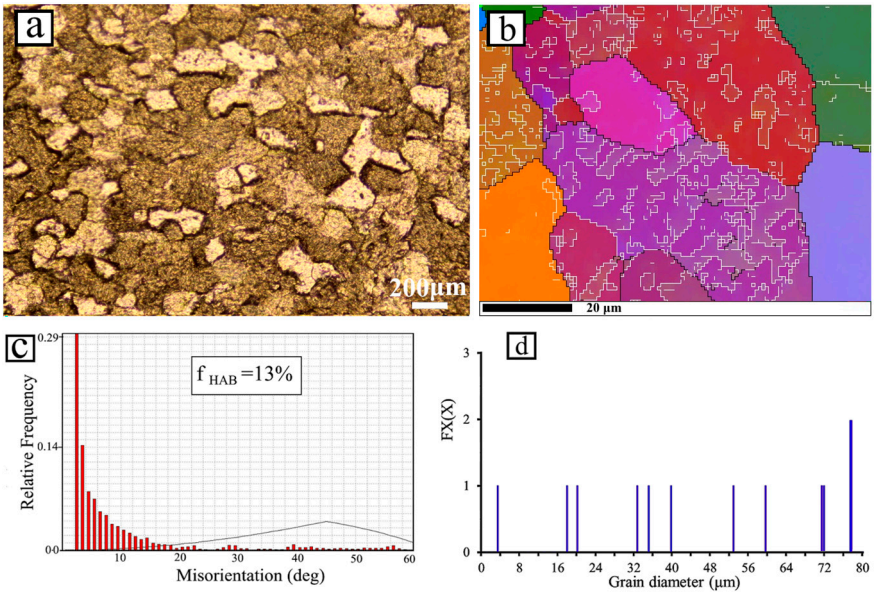

Figure 3. Optical micrographs (**a**), EBSD maps (**b**), high angle fraction diagrams (**c**), and grain size distribution (**d**) in annealed AA1100 aluminium alloy.

The annealed Al alloy's maximum temperature (499.7 °C) is about 2.5% higher than that of the wrought alloy (488.2 °C). Due to its prior thermo-mechanical treatments, which result in higher dislocation density, the wrought aluminium alloy exhibits superior mechanical strength and thermal resistance. As a result, the material experienced a less intense materials flow during FSP and showed a lower peak temperature compared to the annealed alloy with higher flowability.

The wrought and annealed AA1100 alloy microstructure after FSP with Al + Fe_2O_3 milled powder mixture was studied by optical microscopy, FE-SEM, and EBSD technique. The outcomes of the study by optical microscopy and FE-SEM are shown in Figure 6. As shown in Figure 6a,c, no agglomerated coarse particles, pores, and other defects are found in the SZs of both FSPed specimens. Furthermore, grains were thoroughly refined to equiaxial grains. FE-SEM images (Figure 6b,d) show particles were uniformly distributed

in the SZs of the specimens. Thus, it can be confirmed that composite material is formed for both samples.

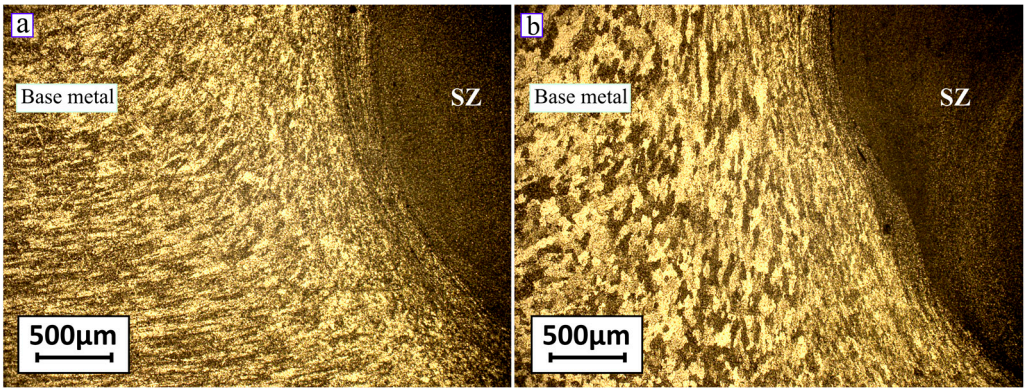

Figure 4. Optical micrographs of the rolled (**a**) and the annealed (**b**) specimens after FSP.

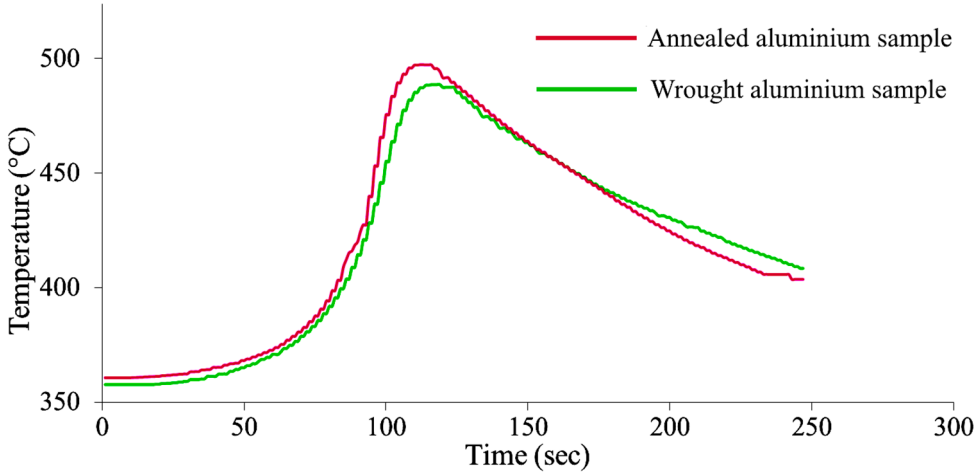

Figure 5. Shows the temperature profiles during the fourth pass FSP for wrought and annealed aluminium samples.

Figure 7 presents XRD patterns of both the rolled and the annealed specimens after FSP with powder addition. Minor phases associated with the crystal structures of $Al_{13}Fe_4$, Al_2O_3, FeO, and Fe_3O_4 were also shown, in addition to peaks dominant to Al. The reaction between Al and Fe_2O_3 occurred during FSP, according to XRD findings. Consequently, in both specimens (rolled and annealed), in situ hybrid nanocomposites were developed. The formation of nanosized reaction products and the associated peak-broadening effect are the causes of low peak-to-background ratios. The iron oxide direction peaks showed that four FSP passes were insufficient to complete the Al-Fe_2O_3 reaction.

The microstructure of the composite sample made from the annealed specimens was examined more closely by transmission electron microscopy (Figure 8). As seen in the picture, different particles are uniformly distributed in the aluminium matrix. Two types of particles can be recognised in the processed composite: elliptical shape and irregular shape. Figure 9 displays the nanometer phases present in the sample made from the annealed specimens, which were taken by scanning transmission electron microscopy. EDS point and elemental mapping analyses were employed to identify the displayed structure.

In this image, both types of particles, ellipticals and irregular shapes, are extant together. According to the EDS point and elemental mapping analyses, it could be concluded that the elliptical-shaped particle is iron–aluminium when the irregular-shaped particle has a core–shell structure. The core structure has a chemical composition of iron-oxygen, surrounded by a shell with a combination of aluminium–oxygen. These results can confirm

the previous findings, especially the X-ray diffraction ones because the outcomes of the XRD pattern showed that iron–aluminium intermetallic compounds, aluminium oxide and iron oxide, are present in the fabricated composite. Additionally, the presence of sediments with a chemical composition of oxygen/aluminium and aluminium/iron is a confirmation of the in situ reaction between aluminium and hematite during the FSP. Eleptical-shaped particles were detected as $Al_{13}Fe_4$ particles with an approximate size of 100 nm. As mentioned earlier, the results of EDS and XRD patterns for these particles are consistent with $Al_{13}Fe_4$ intermetallic composition. It was also found that the irregular-shaped particles are α-Al_2O_3 and Fe_3O_4 particles (Figure 9). During the FSP, the rotating tool breaks and crushes the initial Fe_2O_3 particles, which will be dispersed into the aluminium matrix. This will encourage the reaction between Fe_2O_3 particles and the aluminium base, resulting in the formation of $Al_{13}Fe_4$ and Al_2O_3 intermetallic compounds as reaction products during the FSP.

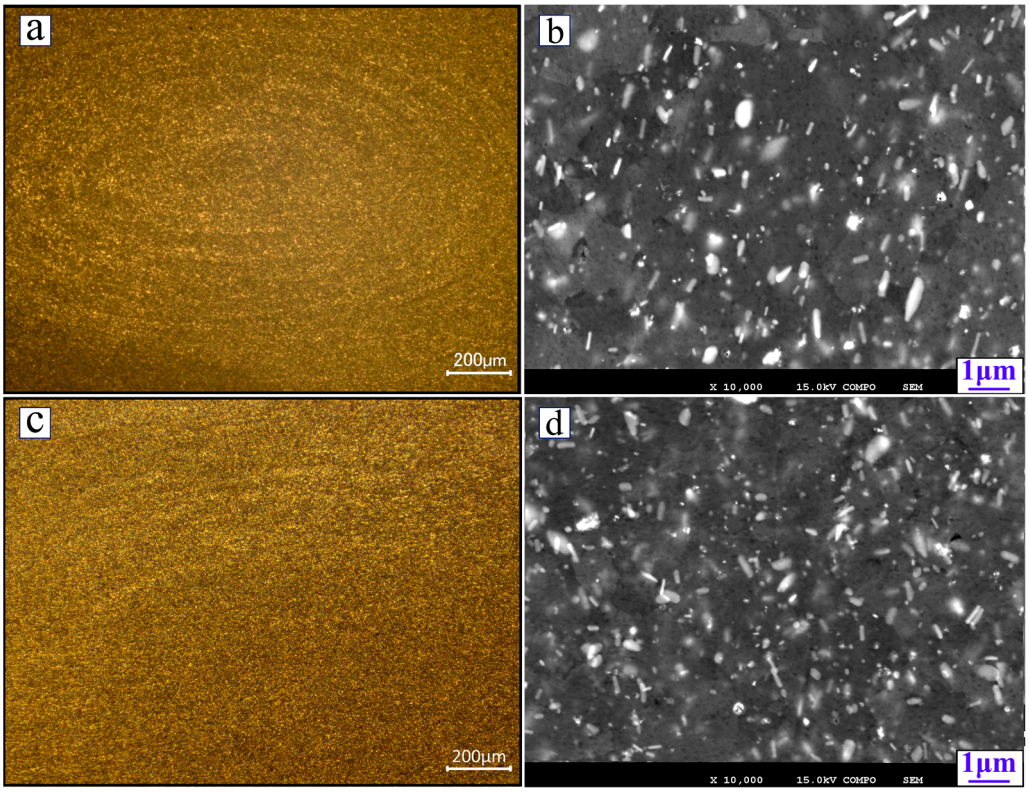

Figure 6. The optical and SEM Micrographs related to the microstructure of the wrought (**a**,**b**) and annealed (**c**,**d**) AA1100 alloy after FSP with Al + Fe_2O_3 milled powder mixture.

Based on our previous studies [19,34], during FSP, the exothermic reaction between Al and Fe_2O_3 can initiate from the heat produced by the rotating tool. In fact, because of the consolidation of high temperature and severe plastic strain related to FSP, the Al–Fe_2O_3 system's exothermic reaction started and advanced. It is also noteworthy that our previous findings indicated that mechanical milling of the powder mixture before FSP enhances the kinetics of the exothermic reaction [34]. Therefore, the amount of in situ products, $Al_{13}Fe_4$ and Al_2O_3, resulting from the reaction increases. Those particles act as reinforcements, and thus the matrix grains will be refined by the pinning mechanism of the grain boundary.

Figure 10 illustrates the EBSD mapping and frequency distribution of grain sizes for the rolled and annealed FSPed specimens with an Al + Fe_2O_3 milled powder mixture. Recrystallised grains of about 3 µm are seen in the wrought alloy SZ (Figure 10a). The FSP zone of the annealed samples (Figure 10b), like that of the wrought alloy, comprises fine recrystallised grains of 2 µm that are slightly smaller than that of the wrought specimens.

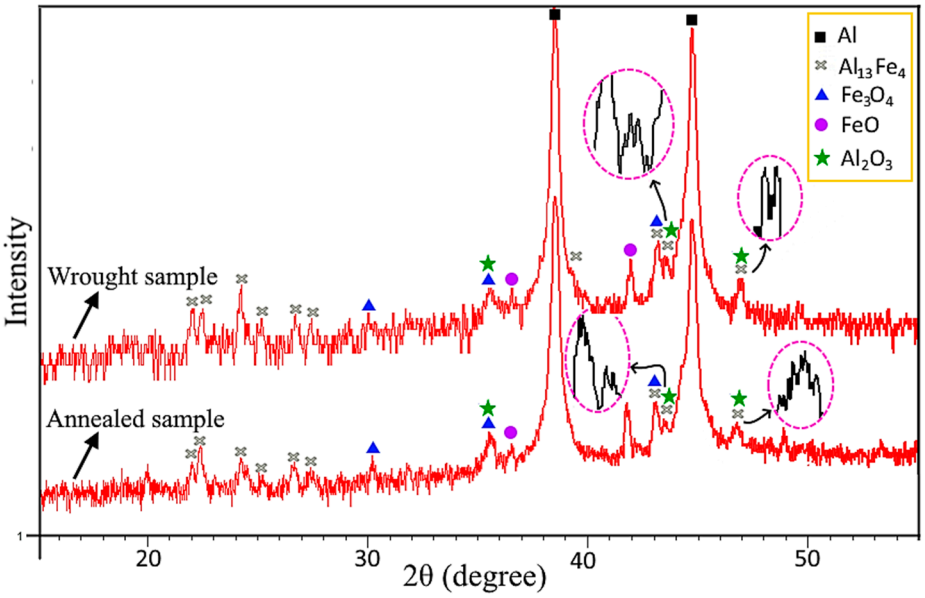

Figure 7. XRD patterns of both the rolled and the annealed specimens after FSP.

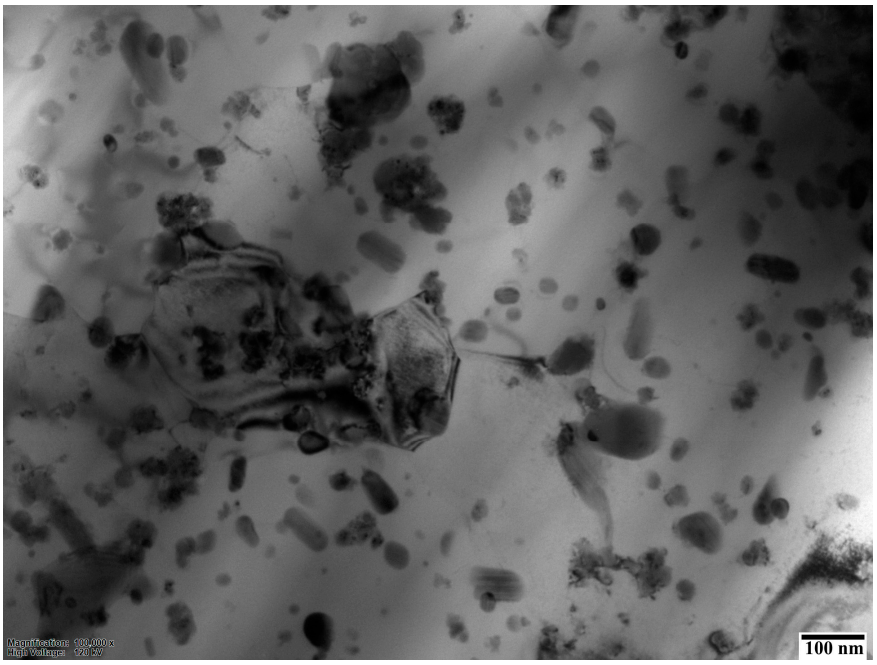

Figure 8. TEM bright field micrograph of the annealed specimens after FSP with powder addition.

Various researchers have investigated mechanisms that lead to grain refinement during FSP [5,8,30,35]. Based on their report and the finding of our previous study, materials have been subjected to hot deformation. As a result, dynamic recovery (DRV) and dynamic recrystallisation (DRX) of the highly distorted grains occur and cause grain refinements. The annealing treatment and the recrystallisation phenomena almost controlled the final microstructure after FSP.

It is known the factors influencing DRX are: (a) stacking fault energy (SEF, γ_{SFE}); (b) initial grain size; (c) thermo-mechanical processing conditions; and (d) second-phase particles [27]. Material stacking fault energy has a considerable impact on the DRX [36]. During hot deformation of materials with high SFE, such as aluminium, due to the effective DRV, CDRX is often observed. Subgrain structures with LAGBs are formed at more significant deformations and gradually transformed into high-angle grain bound-

aries (HAGBs) [37]. During high-temperature deformation, it is usual to observe the development of a homogeneous microstructure [27]. As a result, the micro-shear and deformation bands become less significant compared to cold deformation. Under these conditions, CDRX occurs by the continuous pile-up of dislocations into LAGBs, which raises their misorientation.

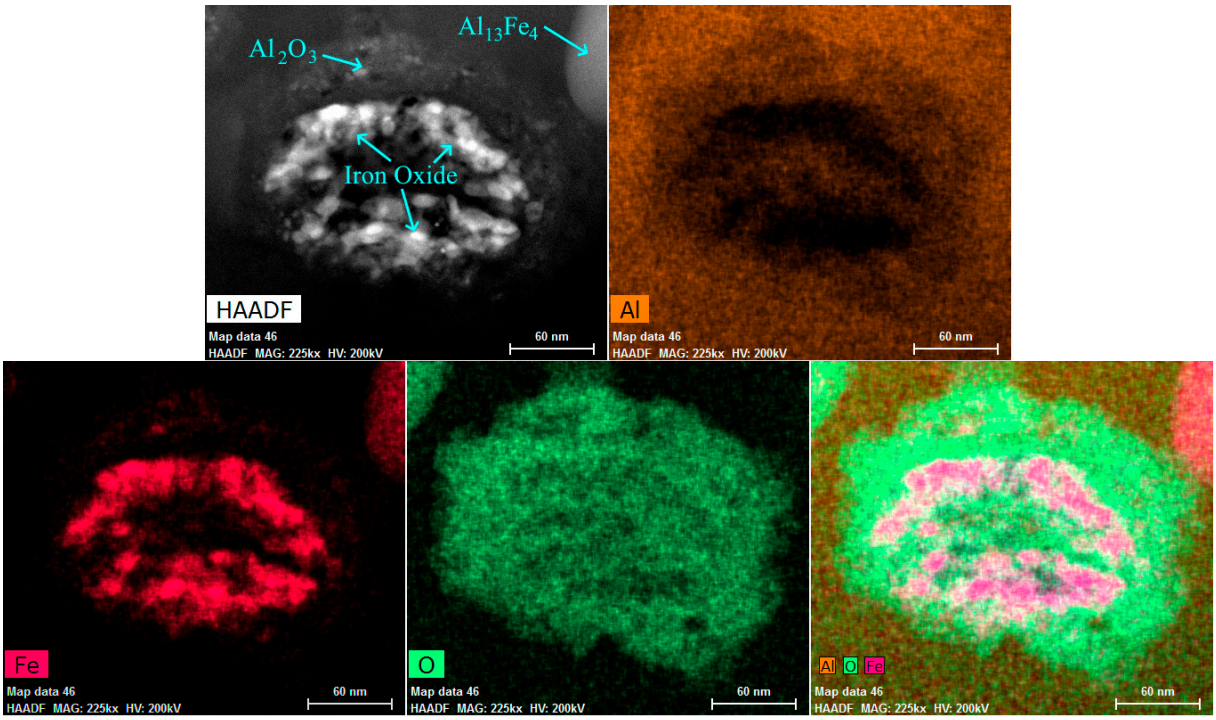

Figure 9. HAADF imaging, EDS mapping, and selected area diffraction pattern of particles in the fabricated hybrid nanocomposite.

In due course, HAGBs are created when misorientation angles exceed a critical value θ_c ($\theta_c = 15°$) [38]. As mentioned above, the nanosized particles ($Al_{13}Fe_4$ and Al_2O_3) are formed during reactive FSP, acting as reinforcements. These particles also have an essential role in recrystallisation. They are inclined to hinder boundary movement and decrease the rate of recrystallisation and grain growth through a Zener pinning mechanism. After a certain deformation level due to the action of small second-phase particles, the (sub)boundaries are pinned. On the other hand, the entrapment of dislocations within boundaries increases the dislocation density, and the lattice's local strain close to particles enhances the fraction of HAGBs. Since in the reactive FSP, precipitation co-occurs during DRX, the driving force of recrystallisation and the Zener pinning mechanism proceed over time. However, as demonstrated in Figure 10, grains are slightly smaller in the nanocomposite fabricated on the annealed base metal compared to the nanocomposite grain size processed on the rolled base metal. Therefore, it can be concluded that, in addition to the effect of γ_{SFE} and nanoparticles on grain refinement, the initial particle size also affects the final structure. As mentioned before, one of the factors influencing microstructure evolution during DRX is the initial grain size. The previous study reveals that the grain boundaries act as primary nucleation sites for the new grains [39,40]. Therefore, fine primary grain size provides more nucleation sites. Under a significant strain deformation, the kinetics of grain refinement can notably accelerate by reducing the initial grain size; therefore, the development of misorientation for LAGBs is quicker [41]. As illustrated in Figure 10, the nanocomposites fabricated on the annealed sample have a finer structure. This observation reveals the influence of pre-stored strain energy on the grain growth after dynamic recrystallisation. During the FSP of rolled alloy, there is competition between the grain structure refinement and recovery mechanisms.

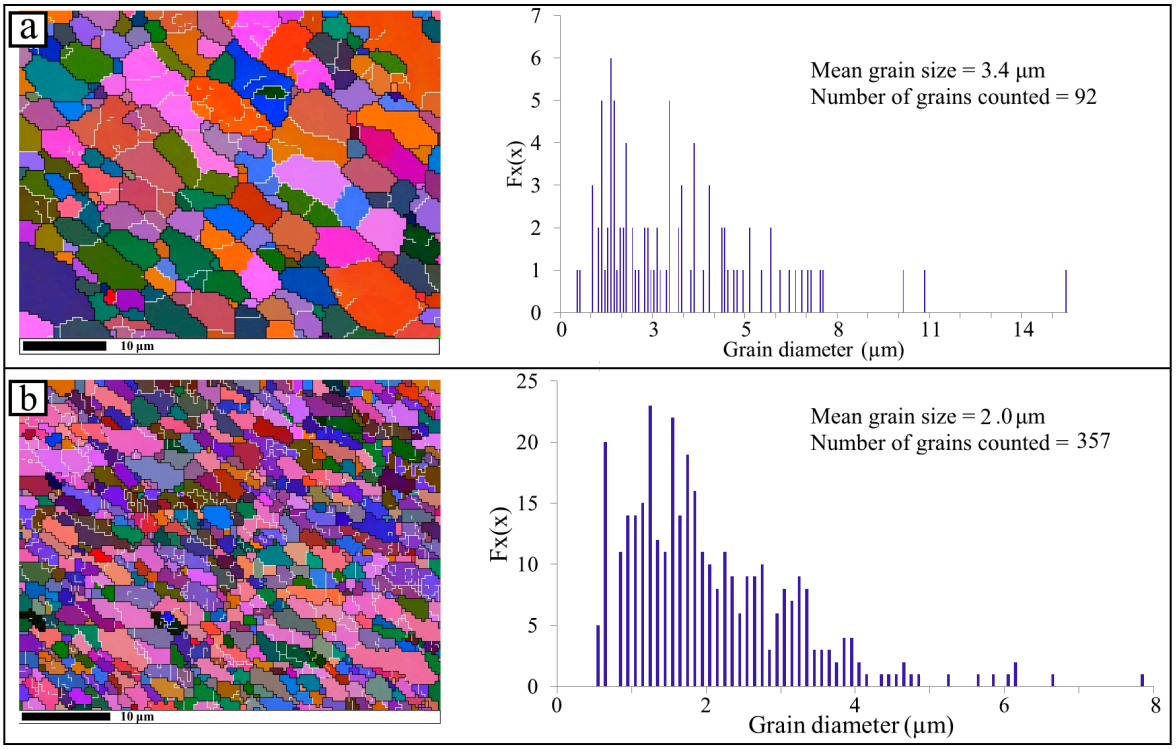

Figure 10. EBSD mapping and frequency distribution of grain sizes for (**a**) the rolled and (**b**) annealed FSPed specimens.

The kernel average misorientation (KAM) or local misorientation histogram of the rolled and annealed specimens following FSP with powder addition is shown in Figure 11. These specimens were obtained in the middle of the cross-section of the samples. KAM is correlated to the average misorientation between a point and its closest neighbours that are also part of the same grain. KAM is connected to misorientation of less than 5°. The local plastic strain in specimens was therefore evaluated using the KAM histogram. According to Figure 11, the annealed specimen had higher kernel values than the rolled sample.

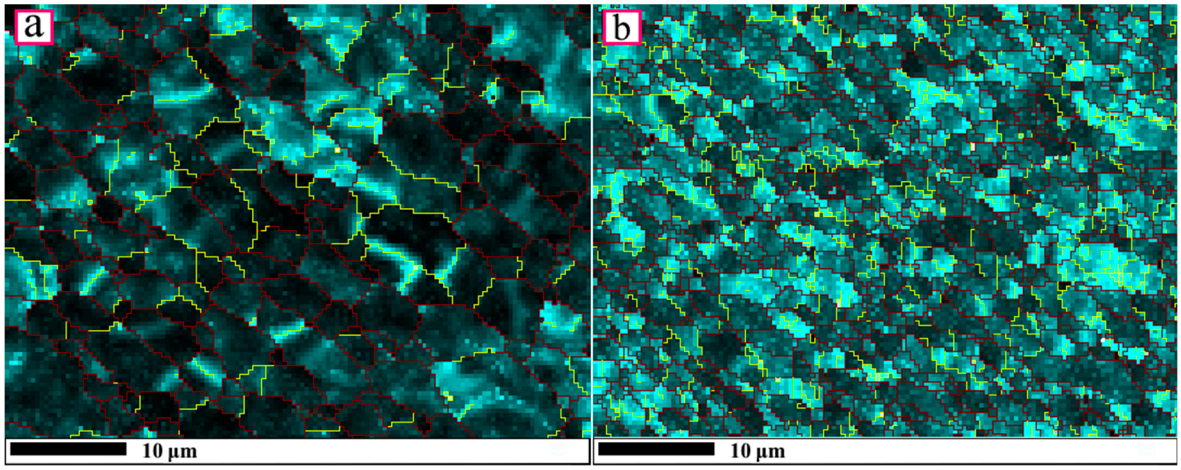

Figure 11. Kernel average misorientation (KAM) or local misorientation histogram of (**a**) the rolled and (**b**) the annealed specimens after FSP.

Figure 12 displays the KAM value versus relative frequency. It is clear that the rolled specimen exhibits the highest relative frequency of low KAM values (less than 0.5). In contrast, the annealed sample demonstrates the highest relative frequency of high KAM

values. The high KAM values in the annealed sample imply that it has a high dislocation density [42]. As a result, it is evident that following FSP, the dislocation density in the annealed specimen gets higher than in the rolled specimen. Intergranular particles pin these dislocations in the hybrid composite grains.

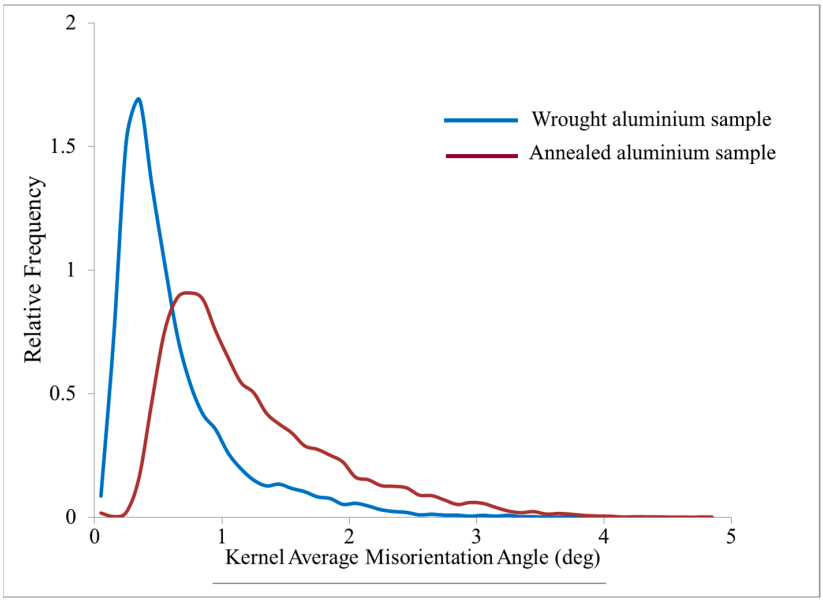

Figure 12. The KAM value vs. relative frequency of the rolled and the annealed specimens after FSP.

The engineering stress–strain curves for the FSPed hybrid composites are shown in Figure 13. The figure shows that the tensile strength for rolled and annealed composites is 146 and 155 MPa, respectively. Therefore, the annealing treatment before FSP resulted in the fabrication of a more refined structure during FSP, which significantly impacts the mechanical properties of composites.

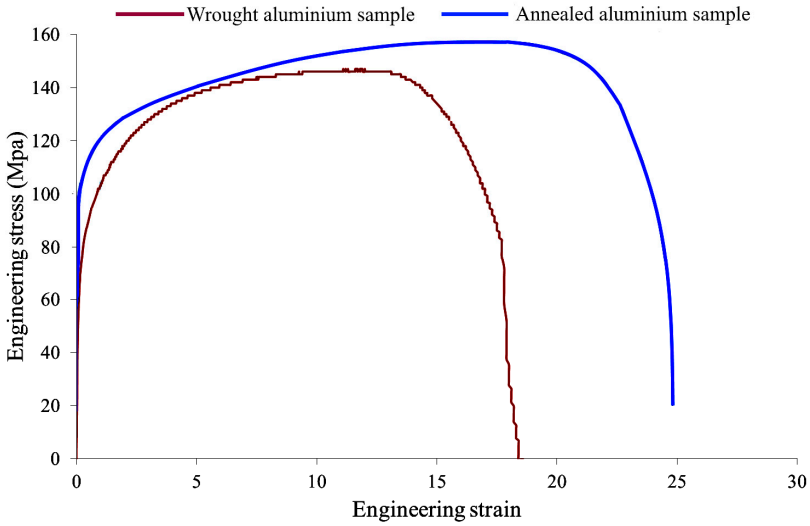

Figure 13. The engineering stress–strain curves for the FSPed hybrid composites.

The microstructure modification during FSP is due to introducing an active powder mixture (Al and Fe_2O_3), and subsequently forming new nanoparticles of Al_2O_3 and $Al_{13}Fe_4$, elastic mismatch mechanisms, and cumulative nucleation of particles. The high ultimate tensile strength of the composite fabricated from the annealed sample is related to the presence of large amounts of reinforcing particles (Al_2O_3 and $Al_{13}Fe_4$), and also the finer grain aluminium matrix and the high dislocation density in this composite.

Figure 14 shows the microhardness along the centerlines of both the rolled and the annealed specimens after FSP with powder addition. It is obvious that the FSP region is harder than the base metal in both specimens. This perception is intently associated with the development of microstructure.

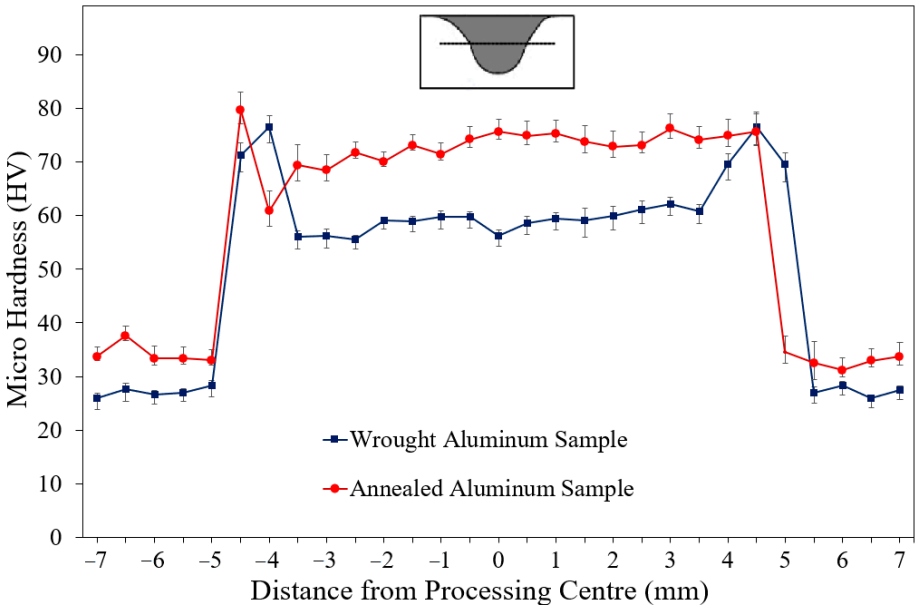

Figure 14. The micro-hardness along the centerlines of both the rolled and the annealed specimens after FSP with powder addition.

The hardness in both samples increased due to microstructure modification, along with an active reaction between aluminium and hematite and, thus, the fabrication of high-hardness products (α-Al_2O_3 and $Al_{13}Fe_4$). However, it is observed that the hardness is higher in the annealed sample. The alloy used in this research (aluminium alloy 1100) is not a precipitation-hardening alloy, so the amount of hardness depends on the grain size, density of dislocations, and hard particles in the matrix (resulting from the active reaction between aluminium and hematite). Intensive grain refinement combined with a higher density of dislocations in this sample resulted in higher hardness in the stir zone. It is noteworthy that it is reported that FSP on this alloy will reduce the density of dislocations in the worked samples. On the contrary, the dislocation density will increase in the annealed samples [43].

According to the Hall–Petch relationship, the grain size strengthening can be illustrated as $kd^{-1/2}$ where d is the grain size, and k is the strengthening coefficient (Yu et al. [44] reported the k = 74 MPa$\sqrt{}$µm for aluminium alloy 1100). In the case of the composite fabricated from an annealed sample, considering the fine aluminium grains size (2 microns) can contribute to the yield strength equal to 52 MPa.

4. Conclusions

In the present study, plates of AA1050 alloy in both annealed and wrought (rolled) conditions were subjected to friction stir processing to produce in situ Al/($Al_{13}Fe_4$ + Al_2O_3) hybrid nanocomposites. The main findings are summarised as follows:

(a) The fabricated hybrid composites by FSP showed a fine-grained Al matrix with a mean grain size of ~2 µm and 3.4 µm for annealed and rolled specimens, respectively;
(b) The initial grain size substantially affects the final microstructures in the friction stir processing. A decrease in the initial grain size can hasten the kinetics of grain refinement considerably under friction stir processing;
(c) The grain size in the composites' FSP zone is affected by the base metal condition, e.g., the rolled and the annealed condition;

(d) KAM histogram showed that after FSP, the dislocation density in the annealed specimen is higher than in rolled samples;
(e) Because of the much finer microstructure and uniform distribution of particles, the hardness and tensile strength of the fabricated composite from annealed specimen were higher.

Author Contributions: Conceptualisation, G.A., S.F.K.-B. and S.L.; methodology, G.A., S.F.K.-B., M.N. and S.L.; investigation, G.A., M.N. and S.L.; writing—original draft preparation, G.A. and S.L.; writing—review and editing, G.A., S.F.K.-B. and S.L.; supervision, S.F.K.-B. and M.N.; data curation, G.A. and S.L. All authors have read and agreed to the published version of the manuscript.

Funding: This research received no external funding.

Data Availability Statement: The data presented in this study are available on request from the corresponding author. The data are not publicly available because it also forms part of an ongoing study.

Conflicts of Interest: The authors declare no conflict of interest.

References

1. Heidarzadeh, A.; Mironov, S.; Kaibyshev, R.; Çam, G.; Simar, A.; Gerlich, A.; Khodabakhshi, F.; Mostafaei, A.; Field, D.P.; Robson, J.D.; et al. Friction stir welding/processing of metals and alloys: A comprehensive review on microstructural evolution. *Prog. Mater. Sci.* **2021**, *117*, 100752. [CrossRef]
2. Ma, Z.Y. Friction stir processing technology: A review. *Metall. Mater. Trans. A* **2008**, *39*, 642–658. [CrossRef]
3. Navazani, M.; Dehghani, K. Fabrication of Mg-ZrO_2 surface layer composites by friction stir processing. *J. Mater. Process. Technol.* **2016**, *229*, 439–449. [CrossRef]
4. Malopheyev, S.S.; Zuiko, I.S.; Mironov, S.Y.; Kaibyshev, R.O. Microstructural Aspects of the Fabrication of Al/Al_2O_3 Composite by Friction Stir Processing. *Materials* **2023**, *16*, 2898. [CrossRef] [PubMed]
5. Chai, F.; Zhang, D.; Li, Y.; Zhang, W. Microstructure evolution and mechanical properties of a submerged friction-stir-processed AZ91 magnesium alloy. *J. Mater. Sci.* **2015**, *50*, 3212–3225. [CrossRef]
6. Izadi, H.; Sandstrom, R.; Gerlich, A.P. Grain growth behavior and Hall–Petch strengthening in friction stir processed Al 5059. *Metall. Mater. Trans. A* **2014**, *45*, 5635–5644. [CrossRef]
7. Papantoniou, I.G.; Markopoulos, A.P.; Manolakos, D.E. A new approach in surface modification and surface hardening of aluminum alloys using friction stir process: Cu-reinforced AA5083. *Materials* **2020**, *13*, 1278. [CrossRef]
8. Malakar, A.; Pancholi, V.; Dabhade, V. Recrystallization and strengthening mechanism in friction-stir-processed Al powder compacts. *J. Mater. Eng. Perform.* **2020**, *29*, 3243–3252. [CrossRef]
9. Abushanab, W.S.; Moustafa, E.B.; Ghandourah, E.I.; Hussein, H.; Taha, M.A.; Mosleh, A.O. Impact of hard and soft reinforcements on the microstructure, mechanical, and physical properties of the surface composite matrix manufactured by friction stir processing. *Coatings* **2023**, *13*, 284. [CrossRef]
10. Hotami, M.M.; Yang, S. Investigation on Micro-Hardness, Surface Roughness and SEM of Nano TiO2/B4C/Graphene Reinforced AA 7075 Composites Fabricated by Frictional Stir Processing. *Crystals* **2023**, *13*, 522. [CrossRef]
11. Iwaszko, J.; Sajed, M. Technological aspects of producing surface composites by friction stir processing—A review. *J. Compos. Sci.* **2021**, *5*, 323. [CrossRef]
12. Muribwathoho, O.; Msomi, V.; Mabuwa, S. Metal Matrix Composite Fabricated with 5000 Series Marine Grades of Aluminium Using FSP Technique: State of the Art Review. *Appl. Sci.* **2022**, *12*, 12832. [CrossRef]
13. Khoshaim, A.B.; Moustafa, E.B.; Alazwari, M.A.; Taha, M.A. An Investigation of the Mechanical, Thermal and Electrical Properties of an AA7075 Alloy Reinforced with Hybrid Ceramic Nanoparticles Using Friction Stir Processing. *Metals* **2023**, *13*, 124. [CrossRef]
14. Roeen, G.A.; Yousefi, S.G.; Emadi, R.; Shooshtari, M.; Lotfian, S. Remanufacturing the AA5052 GTAW welds using friction stir processing. *Metals* **2021**, *11*, 749. [CrossRef]
15. Mondal, S. Aluminum or its alloy matrix hybrid nanocomposites. *Met. Mater. Int.* **2021**, *27*, 2188–2204. [CrossRef]
16. Patil, N.A.; Pedapati, S.R.; Mamat, O.B. A review on aluminium hybrid surface composite fabrication using friction stir processing. *Arch. Metall. Mater.* **2020**, *65*, 441–457.
17. Bodunrin, M.O.; Alaneme, K.K.; Chown, L.H. Aluminium matrix hybrid composites: A review of reinforcement philosophies; mechanical, corrosion and tribological characteristics. *J. Mater. Res. Technol.* **2015**, *4*, 434–445. [CrossRef]
18. Petrović, J.; Mladenović, S.; Marković, I.; Dimitrijević, S. Characterization of Hybrid Aluminum Composites Reinforced with Al2O3 Particles and Walnut-shell Ash. *Mater. Technol.* **2022**, *56*, 115–122. [CrossRef]
19. Azimi-Roeen, G.; Kashani-Bozorg, S.F.; Nosko, M.; Švec, P. Reactive mechanism and mechanical properties of in-situ hybrid nanocomposites fabricated from an Al–Fe_2O_3 system by friction stir processing. *Mater. Charact.* **2017**, *127*, 279–287. [CrossRef]
20. AzimiRoeen, G.; Kashani-Bozorg, S.F.; Nosko, M.; Lotfian, S.J.M.; International, M. Mechanical and Microstructural Characterization of Hybrid Aluminum Nanocomposites Synthesized from an Al–Fe_3O_4 System by Friction Stir Processing. *Met. Mater. Int.* **2020**, *26*, 1441–1453. [CrossRef]

21. Khodabakhshi, F.; Simchi, A.; Kokabi, A.; Sadeghahmadi, M.; Gerlich, A.P. Reactive friction stir processing of AA 5052–TiO_2 nanocomposite: Process–microstructure–mechanical characteristics. *Mater. Sci. Technol.* **2015**, *31*, 426–435. [CrossRef]
22. Madhu, H.; Ajay Kumar, P.; Perugu, C.S.; Kailas, S.V. Microstructure and mechanical properties of friction stir process derived Al-TiO_2 nanocomposite. *J. Mater. Eng. Perform.* **2018**, *27*, 1318–1326. [CrossRef]
23. Chen, C.; Kao, P.; Chang, L.; Ho, N.J. Effect of processing parameters on microstructure and mechanical properties of an Al-$Al_{11}Ce_3$-Al_2O_3 in-situ composite produced by friction stir processing. *Acta Mater.* **2010**, *41*, 513–522. [CrossRef]
24. Kraiklang, R.; Onwong, J.; Santhaweesuk, C. Multi-performance characteristics of AA5052+ 10% SiC surface composite by friction stir processing. *J. Compos. Sci.* **2020**, *4*, 36. [CrossRef]
25. You, G.; Ho, N.; Kao, P. The microstructure and mechanical properties of an Al–CuO in-situ composite produced using friction stir processing. *Mater. Lett.* **2013**, *90*, 26–29. [CrossRef]
26. Gourdet, S.; Montheillet, F. A model of continuous dynamic recrystallization. *Acta Mater.* **2003**, *51*, 2685–2699. [CrossRef]
27. Huang, K.; Logé, R.E. A review of dynamic recrystallization phenomena in metallic materials. *Mater. Des.* **2016**, *111*, 548–574. [CrossRef]
28. Su, J.-Q.; Nelson, T.W.; Sterling, C.J. Microstructure evolution during FSW/FSP of high strength aluminum alloys. *Mater. Sci. Eng. A* **2005**, *405*, 277–286. [CrossRef]
29. Prangnell, P.; Bowen, J.R.; Apps, P.J. Ultra-fine grain structures in aluminium alloys by severe deformation processing. *Mater. Sci. Eng. A* **2004**, *375*, 178–185. [CrossRef]
30. Rao, A.; Ravi, K.; Ramakrishnarao, B.; Deshmukh, V.; Sharma, A.; Prabhu, N.; Kashyap, B. Recrystallization phenomena during friction stir processing of hypereutectic aluminum-silicon alloy. *Metall. Mater. Trans. A* **2013**, *44*, 1519–1529. [CrossRef]
31. Manshadi, A.D. Evolution of Recrystallization During and following Hot Deformation. Ph.D. Thesis, Deakin University, Burwood, Australia, 2007.
32. Sakai, T.; Belyakov, A.; Kaibyshev, R.; Miura, H.; Jonas, J.J. Dynamic and post-dynamic recrystallization under hot, cold and severe plastic deformation conditions. *Prog. Mater. Sci.* **2014**, *60*, 130–207. [CrossRef]
33. Derby, B. The dependence of grain size on stress during dynamic recrystallisation. *Acta Metall. Mater.* **1991**, *39*, 955–962. [CrossRef]
34. Azimi-Roeen, G.; Kashani-Bozorg, S.F.; Nosko, M.; Nagy, Š. Formation of Al/($Al_{13}Fe_4$+ Al_2O_3) Nanocomposites via Mechanical Alloying and Friction Stir Processing. *J. Mater. Eng. Perform.* **2018**, *27*, 471–482. [CrossRef]
35. Khodabakhshi, F.; Simchi, A.; Kokabi, A.; Gerlich, A.; Nosko, M. Effects of stored strain energy on restoration mechanisms and texture components in an aluminum–magnesium alloy prepared by friction stir processing. *Mater. Sci. Eng. A* **2015**, *642*, 204–214. [CrossRef]
36. Zhou, L.; Chen, W.; Feng, S.; Sun, M.; Xu, B.; Li, D. Dynamic recrystallization behavior and interfacial bonding mechanism of 14Cr ferrite steel during hot deformation bonding. *J. Mater. Sci. Technol.* **2020**, *43*, 92–103. [CrossRef]
37. Xu, C.; He, H.; Xue, Z.; Li, L. A detailed investigation on the grain structure evolution of AA7005 aluminum alloy during hot deformation. *Mater. Charact.* **2021**, *171*, 110801. [CrossRef]
38. Kaibyshev, R.; Shipilova, K.; Musin, F.; Motohashi, Y. Continuous dynamic recrystallization in an Al–Li–Mg–Sc alloy during equal-channel angular extrusion. *Mater. Sci. Eng. A* **2005**, *396*, 341–351. [CrossRef]
39. Azimi-Roeen, G.; Kashani-Bozorg, S.F.; Nosko, M.; Orovcik, L.; Lotfian, S. Effect of multi-pass friction stir processing on textural evolution and grain boundary structure of Al–Fe_3O_4 system. *J. Mater. Res. Technol.* **2020**, *9*, 1070–1086. [CrossRef]
40. Azimi-Roeen, G.; Kashani-Bozorg, S.F.; Nosko, M.; Orovcik, L. EBSD investigation of Al/($Al_{13}Fe_4$+ Al_2O_3) nanocomposites fabricated by mechanical milling and friction stir processing. *J. Microsc.* **2018**, *270*, 3–16. [CrossRef]
41. Belyakov, A.; Tsuzaki, K.; Miura, H.; Sakai, T. Effect of initial microstructures on grain refinement in a stainless steel by large strain deformation. *Acta Mater.* **2003**, *51*, 847–861. [CrossRef]
42. Mohtadi-Bonab, M.; Eskandari, M.; Szpunar, J. Texture, local misorientation, grain boundary and recrystallization fraction in pipeline steels related to hydrogen induced cracking. *Mater. Sci. Eng. A* **2015**, *620*, 97–106. [CrossRef]
43. Saito, N.; Shigematsu, I.; Komaya, T.; Tamaki, T.; Yamauchi, G.; Nakamura, M. Grain refinement of 1050 aluminum alloy by friction stir processing. *J. Mater. Sci. Lett.* **2001**, *20*, 1913–1915. [CrossRef]
44. Yu, C.; Kao, P.; Chang, C. Transition of tensile deformation behaviors in ultrafine-grained aluminum. *Acta Mater.* **2005**, *53*, 4019–4028. [CrossRef]